



An Adjustable-Rate User-Printable Rain Gauge Calibrator

Matthew Tippett-Vannini¹, Paul Gaspar², Aiden Hosford², John Selker^{1,2}

¹Biological and Ecological Engineering, Oregon State University, Corvallis, 97330, United States of America

²OPEnS Lab, Oregon State University, Corvallis, 97330, United States of America

Correspondence to: tippettm@oregonstate.edu

Abstract. Accurate precipitation measurement is essential. However, calibration of field-deployed rain gauges remains a challenge. Many methods require laboratory conditions, costly commercial equipment, or instruments designed for specific rain gauges, which cannot accommodate smaller-diameter gauges.

We introduce the **Adjustable-Rate 3D Printed Rain Gauge Calibrator (AR3D)**, a low-cost, open-source device designed for *in situ* calibration of rain gauges.

The AR3D introduces three innovations: (1) an adjustable screw valve, enabling flow rate tuning from $0.15 - 16 \text{ mL min}^{-1}$, accommodating the lower flow rates needed for smaller rain gauges; (2) a compact and durable design developed with low-volume reservoirs and elimination of degradable parts; and (3) an integrated pyranometer cover to generate automatic calibration event signals.

We evaluated the AR3D using gravimetric tests, constant-rate stability tests, device-to-device equivalence tests, and field comparisons. Laboratory gravimetric tests of the AR3D demonstrate its ability to deliver volumes of water accurately with an average error of 0.11% (comparable to ISO Class B tolerances for plastic volumetric flasks) at flow rates within $\pm 5\%$ equivalence across independent devices, with a coefficient of variation (CV) below 5%. The AR3D has been successfully deployed to weather stations in both Kenya and the United States. Field validation of the AR3D with a single setting resulted in a flow rate CV of 8.7%. The AR3D enabled identification of properly functioning rain gauges, as well as an under-reporting station. The total cost of material and labor to build an AR3D is approximately USD 12.

Introduction

Reliable rainfall measurement is essential for hydrologic modeling, agricultural management, and ecological and climate research. Despite this, vast regions of the world remain sparsely monitored, especially in the Global South (Dinku, 2019). One approach to this challenge has been larger measurement networks, incorporating relatively low-cost stations, and citizen science (Sánchez-Quispe *et al.*, 2023; van de Giesen *et al.*, 2014).

However, accurate rain gauge calibration remains a challenge for climate and weather monitoring networks. Despite extensive scientific efforts, calibration protocols are not consistently implemented, leading to decreases in the quality of measurements, propagation of errors, and increased uncertainty in modeling, forecasting, and management (Segovia-Cardozo *et al.*, 2023).



Rainfall monitoring networks employ multiple types of rain gauges, including drip counters, weighing gauges, and the most common type, tipping bucket gauges (Ochoa-Rodriguez et al., 2019). Calibration is essential for all rain gauges, but it is especially consequential for networks integrating low-cost sensors, where factory calibration should be verified before installation (Krüger et al., 2024). For tipping bucket gauges, including both low-cost and professional-grade instruments, dynamic calibration, in which a known volume is delivered at a controlled constant flow rate, is required to compensate for spillage error (Ciach, 2003; Vasvári, 2005). Dynamic calibration of drip counter rain gauges has also been shown to be effective in identifying measurement errors (Stagnaro et al., 2021). Despite their effectiveness, calibrations are typically limited to laboratory settings (Stagnaro et al., 2021; Humphrey et al., 1997; Liao et al., 2021). As a result, these calibrations are time-consuming and costly, and they require instruments to be taken offline and removed from the field for laboratory testing.

Commercial *in situ* dynamic calibrators are available (e.g., RM Young 52260, Nova Lynx 260-2595, Kisters FCD), but these tend to be costly, do not provide high volumetric accuracy without an external weighing tool, and are often designed to fit specific gauges with flow rates incompatible with smaller-diameter gauges. Such constraints, especially cost, hinder their applicability in dense monitoring networks, citizen science initiatives, and low-resource settings (Muller et al., 2015).

Low-cost and open-source devices for *in situ* calibration have been made to address these limitations, notably the 3D calibrator proposed by Lopez Alcala et al. (2019). While these efforts demonstrate the feasibility of inexpensive calibration devices, challenges remain in achieving precise flow control, volumetric accuracy, low-complexity construction, and ease of use under field conditions.

Building upon the 3D calibrator of Lopez Alcala et al. (2019), henceforth referred to as the 3D.1, our “Adjustable-Rate 3D-Printed Rain Gauge Calibrator”, (AR3D hereafter), is a low-cost, modifiable, adjustable, and field-deployable device designed to address these challenges. The AR3D introduces several design modifications to improve functionality and convenience. Key improvements found in the AR3D are:

- 55 • the reduction in scale of both the volumetric flask and the calibration device to be compatible with smaller-size rain gauges
- the inclusion of a set screw to allow adjustment of flow rate
- the change of printing material and printing method
- the removal of O-rings
- the inclusion of a built-in calibration event signal.

60 The AR3D was initially designed for and tested on the METER Group’s ATMOS 41, a drip counter rain gauge with a 9.3 cm funnel diameter, selected as a representative research-grade instrument commonly used in monitoring networks. However, the AR3D can be easily modified to fit any rain gauge using the adaptable design files provided, including the use of a larger volume water source. This design philosophy aligns with calls for open and adaptable instrumentation in environmental monitoring (Pearce, 2016). By enabling dynamic calibration *in situ*, the AR3D supports more frequent quality control without interrupting ongoing precipitation measurements, thereby improving data quality (Tapiador et al., 2017).



This document details the design of the AR3D, materials and methods of construction, methods of evaluation, and the results of those tests. Open-source and modifiable design files for AR3D can be found in the appendix material.

2. Device Design

70 2.1 Background on Calibrators

The AR3D, like the 3D.1, uses a Mariotte bottle to passively provide a constant flow rate, (Mariotte, 1717, as cited in McCarthy, 1934). The principle of the Mariotte bottle holds the hydraulic gradient constant.

Applying the Hagen-Poiseuille equation, with the assumptions of laminar flow (Poiseuille, 1841, as cited in Pfitzner, 1976) and positioning the air entry tube (h_{air}) at a constant distance (L) from the water outlet (h_{out}), the hydraulic gradient (∇H) and 75 thus the flow (Q) are constant, Eq. (1):

$$Q = \frac{\pi r^4 \nabla H}{8\eta} = c \nabla H = c \left(\frac{\Delta h}{\Delta L} \right) = c \left(\frac{h_{out} - h_{air}}{L} \right) = c \left(\frac{L}{L} \right) = \text{Constant ,} \quad (1)$$

where r is the radius of the tube, η is the dynamic viscosity of the fluid, $c = \frac{\pi r^4}{8\eta}$ (a constant in this case), ∇H is the hydraulic gradient, ΔL is the flow path, and Δh is the hydraulic head difference.

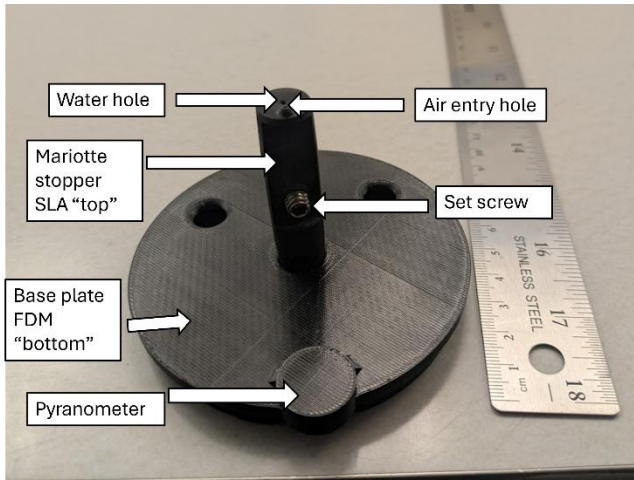
Both the 3D.1 and the AR3D use a polypropylene volumetric flask as the reservoir into which the calibrator is inserted.

80 2.2 Changes from the 3D.1

The 3D.1 calibrator is designed with three flow rates, printed using three independent Mariotte stoppers with progressively larger radii to accommodate increasing flow. While this range of flow rates is effective for many larger rain gauges, the slowest rate was too high for small rain gauges, such as the ATMOS 41.

Furthermore, while the flow rates of the 3D.1 can be modified prior to printing, they do not allow for any adjustments once 85 the device has been printed. The AR3D includes a set screw which allows for *in situ* adjustments of flow rate, as shown in Fig. 1.

Additional changes from the 3D.1 include: the removal of O-rings, the addition of a pyranometer cover, and a change in material.



90 **Figure 1 Elements of the AR3D: The Mariotte stopper printed with SLA, the base plate printed with fused deposition modeling (FDM), the set screw, the pyranometer cover, and the air and water holes.**

2.2.1 Reduced Size

The original goal of this project was to select the slowest flow specified from the 3D.1 and reduce the size of the volumetric flask, from 500 mL to 100 mL, to reduce the time needed for a full calibration. This necessitated reducing the size of the 95 neck of the calibrator to fit the smaller flask. During the modification process, it was observed that the ATMOS 41's operational range for precipitation was 0-400 mm hr^{-1} , however, it only had a $\pm 5\%$ accuracy for rates of ≤ 50 mm hr^{-1} (See Appendix B). The 3D.1's slowest designed rainfall rate (when considering the 9.3 cm diameter of the ATMOS 41) was ~ 148 mm hr^{-1} , roughly three times higher than the upper limit of the higher accuracy range for the ATMOS 41. Another source of concern was that the slowest rate (147 mm hr^{-1}) had the highest variability in flow rate measurements for the 3D.1, with a 100 coefficient of variation of 25.5%, compared to 3.9%, 2.2% and 1.8% for the 220 mm hr^{-1} , 450 mm hr^{-1} , and 740 mm hr^{-1} rates respectively.

The AR3D was redesigned to fit the 100 mL volumetric flasks and has reduced radii for the air and water holes in the Mariotte stopper.

2.2.2 Adjustable Flow Rate

105 The most significant change from the 3D.1 to the AR3D is the introduction of an adjustable-rate screw valve, which can further reduce the effective area of the water hole. While the 3D.1 was modifiable at the design stage, once printed, the rate could not be changed. The addition of the adjustable set screw means that the flow rate can be changed prior to any calibration event.



2.2.3 Removal of O-rings

110 The 3D.1 contained O-rings to ensure a good seal with the volumetric flask. During early testing of the 3D.1 we found these O-rings to have quickly hardened and cracked. Because the calibrators are intended to be used outside in remote areas and in sunlight, conditions which can cause an accelerated breakdown of rubber parts and difficulties in finding replacements, the AR3D has been designed not to need O-rings to form the seal. The top of the AR3D is tapered at the same angle as the volumetric flask to ensure a good seal.

115 **2.2.4 Addition of Pyranometer Cover**

Dynamic calibration may be misinterpreted as a rain event, if not properly flagged by operators. While care must be taken to flag the data and take notes, as an extra precaution the AR3D has an automated calibration event signal incorporated into the device. An opaque cover placed over the pyranometer sensor notch (as shown in Fig. 1) blocks incident sunlight for the duration of the calibration event, resulting in an apparent and sudden drop in recorded radiation by the pyranometer sensor.

120 This combination of an abrupt drop in radiation during a short rainfall event can then be flagged as a calibration event. The drop in radiation would be so extreme (ideally 0 W m^{-2}) as not to be confused with cloud cover. This addition is specific to the ATMOS 41 but could be modified or removed for other rain gauges.

2.2.5 Change of Material

125 The 3D.1 was printed using fused deposition modeling (FDM) with Acrylonitrile Butadiene Styrene (ABS) plastic filament and printed using both a Lulzbot TAZ5 and a Fusion3 F400 printer.

ABS filament is generally considered a good engineering plastic both for weight and strength. However, the FDM-printed 3D.1 required drilling to reach ideal specifications, as the printer's resolution was too coarse.

130 In our early attempts to use a modified version of the 3D.1 for small diameter rain gauges, sealed-in glass capillary tubes were also introduced. While these did improve the accuracy of the measurements, the labor costs of cutting and sealing capillary tubes, in addition to drilling, were high.

For these reasons, the upper section of the AR3D was printed with stereolithography (SLA). The calibrators were SLA 3D printed using an Anycubic Photon Mono X printer, which uses a UV light source matrix (consisting of quartz lamp beads) that passes through an 8.9 in 4K monochrome LCD to cure "pixels" of resin on a plastic (FEP) release film. The resin used was Anycubic Water Washable Black 2.0, with the pre-print operations taking place in Lychee Slicer with the official $50\mu\text{m}$ settings for the given resin being used (specifically 5 burn-in layers with a 25-second exposure time, $50\mu\text{m}$ normal layer thickness with a 2.8-second exposure time.) Once the STL files were imported into the slicer, they were rotated 55 degrees on the x-axis, after which supports were autogenerated by the slicer and manually adjusted to ensure optimal printing. Then the parts were duplicated (so that more could be printed simultaneously) and the sliced file was exported to UVTools for layer-by-layer analysis to ensure that there were no unsupported overhangs, resin traps, or suction cups.



140 For the FDM printed base, PETG was the chosen filament, largely due to its relatively higher (than PLA) softening temperature, since PLA (the alternative) will deform at temperatures around 120 degrees Fahrenheit (i.e. if left inside of a vehicle during high temperature weather.) The FDM printer used was the Bambu Labs X1C with a 0.4mm nozzle and 1.75mm filament. The print profile for this material and printer is Bambu Labs provided generic PETG profile.

2.3 Design Specifications of the AR3D

145 The design files for the AR3D can be found in the appendix materials. Additionally, the build specifications are also shown in Table 1:

Table 1: AR3D Build Specifications	
Attribute	Value
Base mass	25.4 g
Base diameter	91 mm
Base height	11 mm
Stopper height (from base)	62 mm
Stopper top diameter	13 mm
Stopper mass	8.5 g
Base plastic	PETG
Stopper plastic	Resin
Pyranometer cutout diameter	13 mm
Water outlet hole diameter	1.6 mm
Air entry hole diameter	0.8 mm
Water outlet capillary tube diameter	1.1 mm

Table 1) Build specifications for the AR3D.

2.4 Cost of AR3D

The AR3D has a slightly higher material cost than the 3D.1 due to the use of SLA printers and inclusion of the set screw.

150 This increased material cost is offset by the reduced labor costs. The total cost of an AR3D is ~USD 12, including purchased items (Table 2). This is comparable to the 3D.1 and both calibrators are far less expensive than commercially available products by approximately an order of magnitude.

Table 2: AR3D Bill of Materials		
Material	Cost per Unit	Total Cost
Resin	USD 21.00 kg ⁻¹	USD 0.18
Filament	USD 21.00 kg ⁻¹	USD 0.50
Volumetric Flask	USD 5.00 unit ⁻¹	USD 5.00
Set screw	USD 0.50 unit ⁻¹	USD 0.50
Allen Key	USD 1.00 unit ⁻¹	USD 1.00
Hourly work (for printing)	USD 20 hour ⁻¹	USD 5.00



Total	-	USD 12.18
-------	---	-----------

Table 2) Materials and associated costs for the AR3D.

3. Methods of Testing and Validation

155 To evaluate the AR3D, we first tested the calibrator under laboratory conditions. We measured time with a stopwatch and mass passing through the AR3D with a 0.01g precision balance. Having both the mass and the time, we calculated the flow rate through the AR3D. Weighing the AR3D (including the flask) before and after measurements allowed for gravimetric measurement of water volume. As the AR3D is designed to be used in field conditions, all tests were conducted using simple tap water.

160 It is useful to relate the output flow rate of the AR3D (mL min^{-1}) to the equivalent rainfall intensity (mm hr^{-1}). For a gauge with a funnel diameter d (cm) and a funnel area, A (cm^2), Eq. (2):

$$A = \pi \left(\frac{d}{2}\right)^2 \quad (2)$$

The delivered flow rate Q (mL min^{-1}) corresponds to a rainfall rate R (mm hr^{-1}) by, Eq. (3):

$$R = \frac{Q*600}{A} \quad (3)$$

165 Where the 600 is for a unit conversion from cm min^{-1} to mm hr^{-1} . For example, a flow rate from the AR3D of 5.7 mL min^{-1} , on the ATMOS 41 (which has a funnel diameter of 9.3 cm) gives an effective rainfall intensity of $\sim 50 \text{ mm hr}^{-1}$.
Following the laboratory tests, we also deployed the AR3D to field-installed weather stations.
All cleaned calibration data derived from testing and used for validation were archived on Zenodo (Tippett-Vannini, 2025).

3.1 Precise Volume Evaluation

170 Ensuring the AR3D can deliver a known volume consistently is essential to dynamic calibration. The major barriers to precise delivery of volume are twofold: 1) precision limitations of the added volume, i.e., the error intrinsic to the volumetric flask reservoir; 2) changes to the mass balance via water entrapment during the calibration. The precision limits of the first are specified by the manufacturer of the flask. To verify mass balance, the AR3D (with the reservoir flask attached) was weighed empty and filled prior to testing and re-weighed after each run to calculate the delivered mass. The delivered 175 quantity was defined gravimetrically as the filled minus the post-calibration mass. This was converted to volume based on the density of water under laboratory temperatures, 0.99 g cm^{-3} for laboratory temperatures of 22°C . Delivered volumes were recorded across replicates ($n=17$) and the mean, median, standard deviation, and CV were calculated to quantify delivery accuracy and precision.



3.2 Slower Rate

180 In addition to delivering a known volume of water, it was necessary to evaluate if the AR3D could deliver slower flow rates, compatible with the ATMOS 41, and much slower than any of the rates from the 3D.1 or commercially available calibrators. Our objective was to reduce the rate to at least be within the ATMOS 41's $\pm 5\%$ accuracy at 50 mm hr^{-1} (5.7 mL min^{-1}).

3.3 Constant Rate

Not only did the flow rate of the AR3D have to be slower, it also was important that the rate was constant. For each 185 calibration run ($n=17$), the delivery was evaluated by first adjusting the set screw to a desired setting and measuring the cumulative mass of water passing through the AR3D at regular time intervals. Settings between 1.6 to 16 mL min^{-1} , were tested to detect if the rates were constant for across a wide range of flow rates. The accumulated mass vs. time measurements were divided into first- and second halves (split at the median). The rate for each half was calculated via a linear regression. We defined the rate drift as the difference between the second-half slope and the first-half slope. We report the summary 190 statistics across all runs, specifically median and width of interquartile range (IQR) of drift, and the percentage of runs that are within a $\pm 10\%$ tolerance band.

3.4 Consistent Measurements (Single Device)

The next test for the AR3D was to confirm that it could deliver consistent and repeatable flow rates. This was tested by 195 adjusting the set screw to a desired rate and repeating the measurements. The coefficient of variation (CV) was then calculated from the repeat measurements.

3.5 Equivalent Measurements Using Independent Devices

To ensure that calibrators can be manufactured to deliver reliable flow rates, we tested independent AR3Ds by first adjusting their rates to be close to one another and then performed a series of paired measurements at that same rate ($n=10$). We recorded the values for each measurement and the device identity and performed two one-sided t-tests (TOST), (Lakens, 200 2017). The equivalence bound was set at $\pm 5\%$.

3.6 Evaluation of the Pyranometer Cover

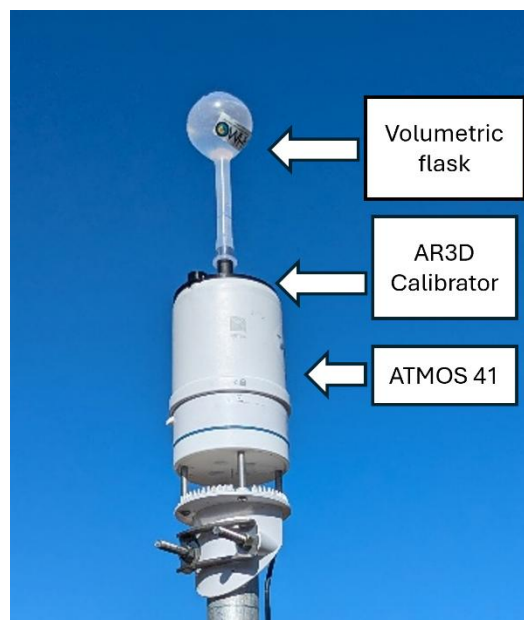
The opaque cover for the pyranometer sensor was evaluated using an ATMOS 41 to log radiation data. The pyranometer data was observed for the duration of a calibration event (~ 15 minutes).

3.7 Field Evaluations

205 The AR3D was deployed to two *in situ* rain gauges in Kenya and one in the United States. Figure 2 shows the AR3D deployed on the ATMOS 41 rain gauge during an *in situ* calibration. Flow rate constancy, consistent measurements,



pyranometer occlusion, as well as volume measured by the rain gauge, were all evaluated. Independent volumetric measurements (apart from carefully filling the volumetric flask) were not conducted due to a lack of precision balances in the field.



210

Figure 2. AR3D field deployment during *in situ* calibration of an ATMOS 41 rain gauge. The AR3D is mounted on the gauge funnel and delivers a controlled calibration volume while the pyranometer occlusion feature provides an automated calibration-event signal.

215 **4. Results**

4.1 Precise Volume

The specifications provided by the volumetric flask manufacturer were ± 0.3 mL ($\pm 0.3\%$). To quantify the water retained by the AR3D, we performed 17 gravimetric measurements using three AR3Ds, and five volumetric flasks. The derived measurements of volume delivered (AR3Ds with full flasks minus post-calibration mass) resulted in a mean of 100.11 mL, a 220 median of 100.12 mL, a standard deviation of 0.11 mL, and a CV of 0.11%. These results indicated that the AR3D performed better within the tolerance of the volumetric flasks and fell within the tolerances of ISO 5215:2022 Class B, however, overall precision is ultimately limited by the reservoir tolerance.



4.2 Slower Rate

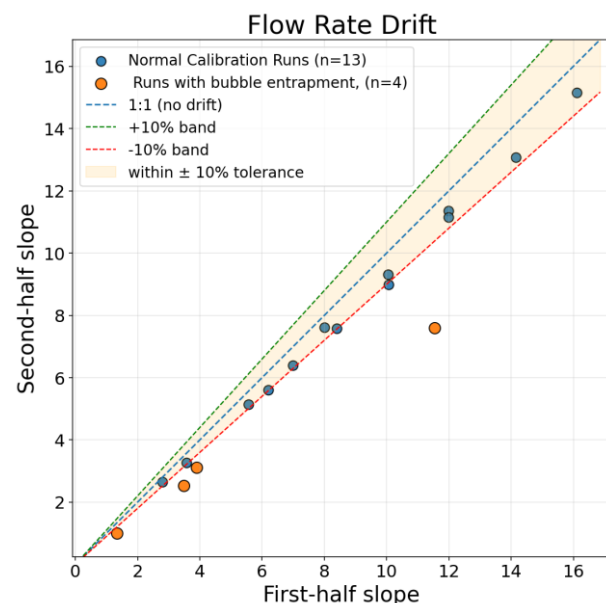
The flow rate of the AR3D can be adjusted to be within the range needed for the ATMOS 41 of 50 mm hr^{-1} (5.7 mL min^{-1}).

225 The calibrator, with its current design files, can achieve flow rates ranging from 0.15 mL min^{-1} to 16 mL min^{-1} , with increments of $\sim 0.15 \text{ mL min}^{-1}$.

4.3 Constant Rate

Across the 17 constant-rate tests, the median drift was -8.5% , the IQR width was 3.7% . 12 of the runs were within the $\pm 10\%$ tolerance band. Four of the five runs which exceeded the $\pm 10\%$ tolerance band also showed evidence of bubble entrapment

230 in the water outlet (near the set screw). When bubble-blocked runs were excluded, the remaining 13 measurements had a median drift of -7.6% , and IQR width of 2.8% (Fig. 3). Twelve of the 13 bubble-free measurements fell within the $\pm 10\%$ tolerance band. Because nominal flowrates differed among tests, percentage drift is summarized using medians and IQRs rather than means.



235 Figure 3) The figure plots the flow rate drift (first-half slope minus second-half slope of a calibration run). The x-axis shows the first-half slopes and the y-axis the second-half slopes. Note that only downward drifts (i.e., negative) are present. Values in orange show evidence of bubble entrapment and present a much larger flow rate drift.

4.4 Consistent Measurements (Single Device)

Repeat measurements of a single device with a constant setting resulted in CVs ranging from 1.3% to 10.87% . For 12 devices measured, the CV for repeat measurements ($n=3$), had a mean of 4.63% , a median of 4.59% , and a standard deviation of 2.8% .



4.5 Equivalent Measurements Using Independent Devices

The TOST analysis was used to evaluate equivalence using multiple paired measurements ($n=10$) of two devices. The equivalence bounds were set at $\pm 5\%$ of the reference means. Both the lower bound test ($p=0.014$) and the upper bound test 245 ($p<0.001$) were statistically significant, $p<0.05$, and we conclude that the two devices can provide statistically equivalent measurements within $\pm 5\%$.

4.6 Evaluation of the pyranometer cover

The pyranometer cover successfully blocked the incident radiation, causing a drop in measured radiation of two orders of magnitude on the first measurement interval for the ATMOS 41 and a reading of 0 W m^{-2} by the second measurement 250 interval.

4.7 Field Evaluations

In all field calibration measurements, the pyranometer cover successfully blocked incoming radiation for the duration of the run. The three runs in the United States were adjusted to the same flow rate and delivered consistent measurements with a mean flow of 3.78 mL min^{-1} , a standard deviation of 0.33 mL min^{-1} , and a CV of 8.74%. The three Kenyan calibrations 255 delivered moderately constant rates with a mean drift of -10.4%, a median drift of -7%, and an IQR of -5.3%; two of the three were within the $\pm 10\%$ tolerance. The volumes from the three runs in Kenya, as measured by the two gauges, were 98.5 mL, 97.7 mL, and 104.6 mL, all within the $\pm 5\%$ error range of the ATMOS 41, confirming that the gauges were functioning correctly. In contrast the volumes measured by the gauge in the United States were 8.33 mL, 26.13 mL, and 39.64 mL indicating that the gauge requires maintenance or recalibration. Because the delivered volume was constant across all field 260 tests (100 mL), field results are expressed as the percentage of delivered volume measured by each gauge (Fig. 4).

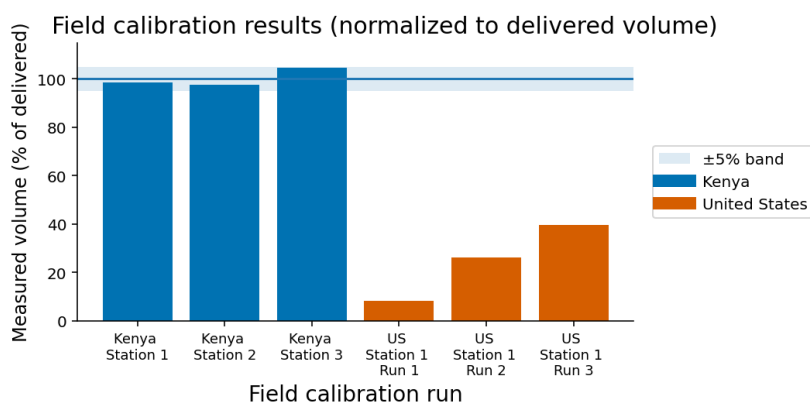


Figure 4) Field calibration run results expressed as the percentage of delivered volume measured by ATMOS 41 rain gauges during six *in situ* calibration runs. The delivered volume was 100 mL for all tests, and the shaded region indicates the $\pm 5\%$ accuracy band. The three Kenyan calibration runs were conducted at three independent stations, and all were within the $\pm 5\%$ band. The three U.S. measurements represent repeated calibration runs at a single station, which consistently under-reported the delivered volume.



5. Discussion

The AR3D is an evolution from the 3D.1. Significant improvements include an adjustable flow rate, extension to slower rates, fittings for smaller volumetric flasks, a pyranometer cover for automated calibration signaling, and a change in material to allow for higher-resolution printing.

While these improvements make a more adaptable device that can be used for a wide range of rain gauges, the straightforward design of the 3D.1 still offers advantages in certain cases. If a user has a high desired flow rate (greater than 16 mL min^{-1}) and adjustments to the flow rate are not necessary, then the simplicity of the 3D.1 might be the better option.

Regardless of calibrator model, printing the Mariotte stopper in SLA is recommended because it removes the drilling required for FDM printing.

While tests of volumetric precision yielded values inside the tolerances of ISO 5215:2022 class B, the overall tolerances are limited by the volumetric flasks used ($\pm 0.3\%$ being outside the class B designation). Nonetheless, the error tolerances were less than 1% and well within the $\pm 5\%$ error of the ATMOS 41. If greater precision is required, higher precision flasks are available, at a substantially greater cost.

A continuing issue with the AR3D, due to the smaller radii of the air and water holes, is air bubble entrapment. This is a likely culprit for the calibrators with higher CV on repeat runs, as well as the case for calibration runs with high flow rate drift. To address this, we recommend giving a gentle squeeze to the “bulb” of the plastic volumetric flask when initiating the calibration. This equates to a transient pressure pulse which can be used to dislodge air bubbles in microfluidic devices, (Pereiro *et al.*, 2019).

Future work could focus on designs which minimize the risk of air entrapment, potentially through wider, yet longer flow paths which may allow air bubbles to escape while still providing the slower flow rate needed for small rain gauges. Improvements to the set screw, perhaps using a carburetor-like needle valve or simply sanding off the cup point, may provide the current level of adjustability with reduced surface roughness, thus lowering the risk of bubble entrapment.

290 6. Conclusions

The AR3D is a continuation of efforts to develop a low-cost, easy-to-use, adaptable rain gauge calibrator. It can deliver precise volumes at sufficiently constant rates. The major improvements it offers are slower potential rates, compatibility with smaller rain gauges, the inclusion of an adjustable set screw allowing for an adjustable flow rate, a pyranometer calibration event signal, removal of degradable parts, and the change in material and printing processes.

Future improvements could include designs to reduce air bubble entrapment, either through wider and longer water outlets or through the incorporation or modification of set screws to reduce surface area susceptible to bubble entrapment.



The AR3D has been shown to be capable of delivering a constant and slower flow rate, as well as repeatable and consistent measurements. The AR3D was deployed to the field on three occasions and successfully identified two well-operating gauges and one requiring maintenance or recalibration.

300 Low-cost and easy-to-use calibration devices, such as the AR3D, can increase the frequency and availability of *in situ* rain gauge calibrations, thus increasing the quality of precipitation data needed for hydrologic modeling, climate and environmental, and land management.

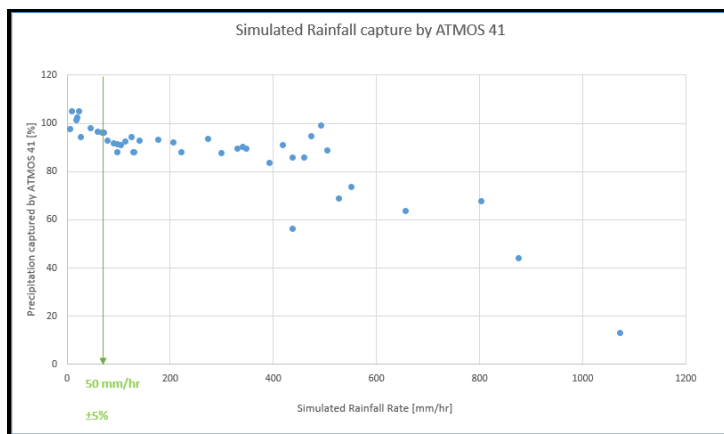
Appendices

Appendix A:

305 Build details can be found at our github:

<https://github.com/OPEnSLab-OSU/OPEnS-Lab-Home/wiki/Adjustable-Rain-Gauge-Calibrator>

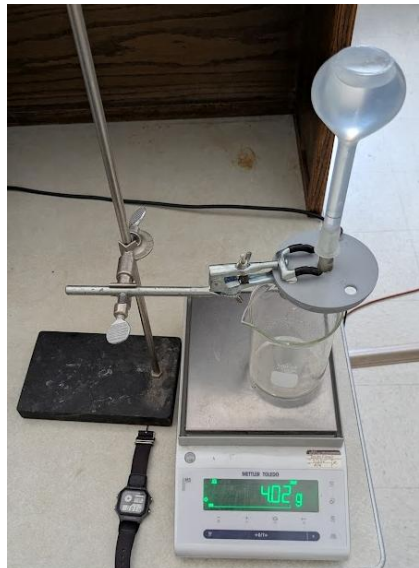
Appendix B:



310 **Figure B1)** Shows the percentage of simulated rain measured by the ATMOS, as a function of rainfall rate. Note that 50 mm hr⁻¹ or less has a ±5% accuracy, rates above 50 mm hr⁻¹ begin to show declining accuracy.

Appendix C:

Photos showing laboratory and field tests of the calibration devices.



315 **Figure C1) Laboratory conditions for evaluating a single AR3D.**

Author Contribution

All authors contributed to the design of the AR3D, Matthew Tippett-Vannini conducted the testing, validation and analysis of the device, Matthew Tippett-Vannini prepared the manuscript with contributions from all authors, all authors reviewed the 320 document, and John Selker was the principal investigator.

Funding

This research received no external funding.

Data Availability

All data supporting this study are publicly available on Zenodo (Tippett-Vannini, 2025):
325 <https://doi.org/10.5281/zenodo.17642189>.

Competing Interests

The authors declare that they have no conflict of interest



Acknowledgements

Special thanks to Gordon Godshalk, Gurpreet Singh, Cara Walter, Travis Becht, Victor Omoit, and the whole OPeNS Lab
330 and TAHMO teams for their help and support.

References

“260-2595 Tipping Bucket Rain Gauge Calibrator.” n.d. NovaLynx Corporation. Accessed December 27, 2025. <https://novalynx.com/store/pc/260-2595-Tipping-Bucket-Rain-Gauge-Calibrator-p1030.htm>.

335 Ciach, G. J. (2003). Local Random Errors in Tipping-Bucket Rain Gauge Measurements. *Journal of Atmospheric and Oceanic Technology*, 20(5), 752–759. [https://doi.org/10.1175/1520-0426\(2003\)20<752:LREITB>2.0.CO;2](https://doi.org/10.1175/1520-0426(2003)20<752:LREITB>2.0.CO;2)

Dinku, T. (2019). Challenges with availability and quality of climate data in Africa. In *Extreme Hydrology and Climate Variability* (pp. 71–80). Elsevier. <https://doi.org/10.1016/B978-0-12-815998-9.00007-5>

340 Humphrey, M. D., Istok, J. D., Lee, J. Y., Hevesi, J. A., & Flint, A. L. (1997). A new method for automated dynamic calibration of tipping-bucket rain gauges. *Journal of Atmospheric and Oceanic Technology*, 14(6), 1513–1519. [https://doi.org/10.1175/1520-0426\(1997\)014<1513:ANMFAD>2.0.CO;2](https://doi.org/10.1175/1520-0426(1997)014<1513:ANMFAD>2.0.CO;2).

345 ISO (International Organization for Standardization). (2022). ISO 5215:2022: Laboratory plastic ware — Volumetric flasks. Geneva, Switzerland: ISO.

350 Krüger, R., Karrasch, P., & Eltner, A. (2024). Calibrating low-cost rain gauge sensors for their applications in Internet of Things (IoT) infrastructures to densify environmental monitoring networks. *Geoscientific Instrumentation, Methods and Data Systems*, 13(1), 163–176. <https://doi.org/10.5194/gi-13-163-2024>

Lakens, D. (2017). Equivalence Tests. *Social Psychological and Personality Science*, 8(4), 355–362. <https://doi.org/10.1177/1948550617697177>

355 Liao, M., Liao, A., Liu, J., Cai, Z., Liu, H., & Ma, T. (2021). A novel method and system for the fast calibration of tipping bucket rain gauges. *Journal of Hydrology*, 597, 125782. <https://doi.org/10.1016/j.jhydrol.2020.125782>

Lopez Alcala, J. M., Udell, C. J., & Selker, J. S. (2019). A user-printable three-rate rain gauge calibration system. *Frontiers in Earth Science*, 7, 338. <https://doi.org/10.3389/feart.2019.00338>

360 McCarthy, E. L. 1934. “Mariotte’s Bottle.” *Science* 80 (2065): 100–100. <https://doi.org/10.1126/science.80.2065.100>.

Montgomery, D. C. (2013). *Design and analysis of experiments* (Eighth edition). John Wiley & Sons, Inc.

365 Muller, C. L., Chapman, L., Johnston, S., Kidd, C., Illingworth, S., Foody, G., Overeem, A., & Leigh, R. R. (2015). Crowdsourcing for climate and atmospheric sciences: Current status and future potential. *International Journal of Climatology*, 35(11), 3185–3203. <https://doi.org/10.1002/joc.4210>

Ochoa-Rodriguez, S., Wang, L.-P., Willems, P., & Onof, C. (2019). A review of radar–rain gauge data merging methods and their potential for urban hydrological applications. *Water Resources Research*, 55(8), 6356–6391. <https://doi.org/10.1029/2018WR023332>.

370 Pearce, J. M. (2016). Return on investment for open source scientific hardware development. *Science and Public Policy*, 43(2), 192–195. <https://doi.org/10.1093/scipol/scv034>



375 Pereiro, I., Khartchenko, A. F., Petrini, L., & Kaigala, G. V. (2019). Nip the bubble in the bud: A guide to avoid gas nucleation in microfluidics. *Lab on a Chip*, 19(14), 2296–2314. <https://doi.org/10.1039/C9LC00211A>

Pfitzner, J. (1976). Poiseuille and his law. *Anaesthesia*, 31(2), 273–275. <https://doi.org/10.1111/j.1365-2044.1976.tb11804.x>

380 *Portable field calibration device | FCD*. (n.d.). KISTERS North America. Accessed December 29, 2025, from <https://products.kisters.net/products/hardware/meteorology/fcd-portable-field-calibration-device>

Rain Gauge Calibrator—Rain Gauge—R.M. Young Company. (n.d.). *R. M. Young Company*. Accessed December 30, 2025, from <https://www.youngusa.com/product/rain-gauge-calibrator/>

385 Sánchez-Quispe, S. T., Madrigal, J., Rodríguez-Licea, D., Domínguez-Mota, F. J., Domínguez-Sánchez, C., Lara-Ledesma, B., (2023). Development of a Low-Cost Automated Hydrological Information System for Remote Areas in Morelia, Mexico. *Water*, 15(22). <https://doi.org/10.3390/w15223888>

390 Segovia-Cardozo, D. A., Bernal-Basurco, C., & Rodríguez-Sinobas, L. (2023). Tipping Bucket Rain Gauges in Hydrological Research: Summary on Measurement Uncertainties, Calibration, and Error Reduction Strategies. *Sensors*, 23(12), 5385. <https://doi.org/10.3390/s23125385>

395 Stagnaro, M., Cauteruccio, A., Lanza, L. G., & Chan, P.-W. (2021). On the use of dynamic calibration to correct drop counter rain gauge measurements. *Sensors*, 21(18), 6321. <https://doi.org/10.3390/s21186321>.

Tapiador, F. J., Navarro, A., Levizzani, V., García-Ortega, E., Huffman, G. J., Kidd, C., Kucera, P. A., Kummerow, C. D., Masunaga, H., Petersen, W. A., Roca, R., Sánchez, J.-L., Tao, W.-K., & Turk, F. J. (2017). Global precipitation measurements for validating climate models. *Atmospheric Research*, 197, 1–20. <https://doi.org/10.1016/j.atmosres.2017.06.021>

400 Tippett-Vannini, M. (2025). AR3D Cleaned Calibration Dataset (Version 1.0) [Data set]. Zenodo. <https://doi.org/10.5281/zenodo.17642189>

405 Vasvári, V. (2005). Calibration of tipping bucket rain gauges in the Graz urban research area. *Atmospheric Research*, 77(1), 18–28. <https://doi.org/10.1016/j.atmosres.2004.12.012>

410 van de Giesen, N., Hut, R., & Selker, J. (2014). The Trans-African Hydro-Meteorological Observatory (TAHMO). *WIREs Water*, 1(4), 341–348. <https://doi.org/10.1002/wat2.1034>